HHS Public Access

Author manuscript

J Infect Dis. Author manuscript; available in PMC 2024 April 22.

Published in final edited form as:

J Infect Dis. 2020 May 11; 221(Suppl 4): S460–S470. doi:10.1093/infdis/jiz564.

Inhibition of Nipah Virus by Defective Interfering Particles

Stephen R. Welch[1], **Natasha L. Tilston**[2], **Michael K. Lo**[1], **Shannon L. M. Whitmer**[1], **Jessica R. Harmon**[1], **Florine E. M. Scholte**[1], **Jessica R. Spengler**[1], **W. Paul Duprex**[2], **Stuart T. Nichol**[1], **Christina F. Spiropoulou**[1]

[1]Viral Special Pathogens Branch, Division of High-Consequence Pathogens and Pathology, National Center for Emerging and Zoonotic Infectious Diseases, Centers for Disease Control and Prevention, Atlanta, Georgia, USA

[2]Center for Vaccine Research, University of Pittsburgh School of Medicine, Pittsburgh, Pennsylvania, USA

Abstract

The error-prone nature of RNA-dependent RNA polymerases drives the diversity of RNA virus populations. Arising within this diversity is a subset of defective viral genomes that retain replication competency, termed defective interfering (DI) genomes. These defects are caused by aberrant viral polymerase reinitiation on the same viral RNA template (deletion DI species) or the nascent RNA strand (copyback DI species). DI genomes have previously been shown to alter the dynamics of a viral population by interfering with normal virus replication and/or by stimulating the innate immune response. In this study, we investigated the ability of artificially produced DI genomes to inhibit Nipah virus (NiV), a highly pathogenic biosafety level 4 paramyxovirus. High multiplicity of infection passaging of both NiV clinical isolates and recombinant NiV in Vero cells generated an extensive DI population from which individual DIs were identified using next-generation sequencing techniques. Assays were established to generate and purify both naturally occurring and in silico-designed DIs as fully encapsidated, infectious virus-like particles termed defective interfering particles (DIPs). We demonstrate that several of these NiV DIP candidates reduced NiV titers by up to 4 logs in vitro. These data represent a proof-of-principle that a therapeutic application of DIPs to combat NiV infections may be an alternative source of antiviral control for this disease.

Keywords

Nipah virus; defective interfering particles; reverse genetics; therapeutic; antiviral

Correspondence: Christina F. Spiropoulou, PhD, Centers for Disease Control and Prevention, 1600 Clifton Road, MS H18-SB, Atlanta, GA, 30333 (ccs8@cdc.gov).

Disclaimer. The findings and conclusions in this report are those of the authors and do not necessarily represent the official position of the Centers for Disease Control and Prevention.

Potential conflicts of interest. All authors: no reported conflicts. All authors have submitted the ICMJE Form for Disclosure of Potential Conflicts of Interest.

The concept of a defective interfering (DI) genome was first proposed in the early 1940s when Preben von Magnus [1] observed decreased influenza virus infectivity when the virus was passaged without dilution, a consequence he suggested was due to “incomplete” viruses competing with authentic virus. In subsequent years, the term defective interfering particle (DIP) was defined as a virion that, although containing the necessary viral proteins for cellular entry, contained an incomplete viral genome that was capable of interfering with standard virus replication [2]. Since then, DIs have been described for numerous RNA virus species, and recent technological advances have allowed researchers to better understand the importance of DIs both in vitro and, more importantly, in vivo. DI genomes are now known to contribute to multiple aspects of viral pathogenesis, including viral interference, persistence, and immune stimulation [3]. The ability to modulate virulence has led to interest in the therapeutic applicability of DIs, with studies showing that DI accumulation in vivo reduces disease severity [4-6], while DI inclusion in vaccines enhances immunogenicity [7-9]. Moreover, experimental DIP treatments have been shown to protect animals from lethal challenge with influenza A virus (IAV) [10-15].

Nipah virus (NiV) is a highly pathogenic paramyxovirus (family *Paramyxoviridae*, genus *Henipavirus*) first described during an outbreak of acute encephalitic disease in humans in both Malaysia and Singapore in 1998–1999 [16]. Since identification, NiV outbreaks have been reported in India and Bangladesh almost yearly [17-19]. NiV outbreaks are characterized by acute respiratory and/or neurological symptoms, frequent person-to-person transmission, and a 70% case fatality rate [20, 21]. Because no vaccines or antivirals are licensed to treat NiV infection, alternative approaches to combat the virus, such as DI treatment, represent attractive research options. A therapeutic DIP may be able to enter the same cellular reservoirs as wild-type virus, reduce viral replication in infected patients, reduce person-to-person transmission by lowering viral load, act as both a prophylactic and post-exposure treatment, and resist generation of escape mutants.

In this study, we used multiple strains of NiV, including recombinant viruses containing mutations thought to facilitate the generation of DIs, to characterize specific DI genomes. Using an innovative next-generation sequencing (NGS) approach, we characterized the population of DI genomes generated, and we showed that predominantly copyback DI species accumulated, although deletion DI were also detected. Copyback DIs are formed during viral genome replication when the viral polymerase jumps from the template RNA genome and rejoins at an RNA genome of the opposite polarity, forming a short ambisense genome with complementary ends of varying lengths. Deletion DIs are formed when the viral polymerase leaves the template RNA genome and rejoins the same template elsewhere, forming a shortened genome with standard leader and trailer ends (reviewed in [22]). We further developed an efficient artificial DIP production system, and we demonstrated that these DIPs directly inhibited NiV replication in vitro. These data represent a proof-of-principle study that the therapeutic application of artificial DIPs to combat NiV infections may offer a viable alternative or supplement to more traditional approaches of infection control.

MATERIALS AND METHODS

Cell Culture

Vero, Vero-E6, and BSR-T7/5 cells were cultured in Dulbecco's modified Eagle's medium (DMEM) supplemented with 5% (v/v) fetal calf serum, nonessential amino acids, 1 mM sodium pyruvate, 2 mM L-glutamine, 100 U/mL penicillin, and 100 μg/mL streptomycin.

Viruses

Wild-type NiV strains used in the passaging experiment were NiV strain Malaysia (NiV-M; GenBank accession no. AF212302) and NiV strain Bangladesh (NiV-B; GenBank accession no. AY988601), passed once on Vero-E6 cells for isolation from clinical sample, and further amplified on Vero cells. Generation of recombinant NiV strain Malaysia (rNiV-M) and rNiV-M expressing the fluorescent protein ZsGreen1 (rNiV-M/ZsG) has been described previously [23]. rNiV-M C- was generated by incorporating T to C nucleotide substitutions in the double initiation codons at genome positions 2429 and 2432 and adding an early stop codon by incorporating a T to A nucleotide substitution at position 2444 (antigenomic sense). rNiV-M D156 encodes a truncated C protein with a deletion of the last 10 C-terminal amino acids of the C open reading frame. The early stop codon mutation was generated by incorporating a T to A nucleotide substitution at position 2894 (antigenomic sense). Neither of these mutations affects the amino acid sequence in the overlapping phosphoprotein (P) open reading frame. All recombinant viruses were rescued on a mixture of BSR-T7/5 and Vero cells and amplified on Vero cells. Viral titers were calculated as 50% tissue culture infective dose ($TCID_{50}$) [24], determined in Vero cells by determining cytopathic effect (CPE) or quantitation of ZsG fluorescence. All recombinant virus work was approved by the Centers for Disease Control and Prevention Institutional Biosafety Committee. All viral stocks were verified by NGS and confirmed to be mycoplasma-free.

NGS and Bioinformatics

Ribonucleic acid was extracted from cell culture supernatants (clarified by low-speed centrifugation) using the manufacturer's TRIzol extraction protocol (Thermo Fisher Scientific) in combination with the DirectZol purification kit incorporating the in-column DNAse step (Zymo Research). RNA sequencing was performed using TrueSeq reagents and analyzed on the MiniSeq system (both from Illumina). Reads were mapped to the appropriate reference genome with in-house scripts by first removing Illumina adaptors (cutadapt version 1.8.3 -a AGATCGGAAGAGCACACGTCTGAACTCCAGTCAC; -A AGATCGGAAGAGCGTCGTGTAGGGAAAGAGTGTAGATCTCGGTGGTCGCCGTATCATT --minimum-length = 1), trimming for low quality bases (prinseq-lite version 0.20.3 -min_qual_mean 25 -trim_qual_right 20 -min_len 50) and mapping to the appropriate reference genome with bwa-mem using default parameters (version 0.7.7). To determine NiV genome breakpoints and reinitiation points, chimeric reads were identified and characterized using a custom script, chimeric_reads.py v3.6.2 [25, 26].

DIP Production Assay

DI expression cassettes were generated as a DNA fragment consisting of the following (in 5′ to 3′ order): BamHI restriction site, T7 promoter, hammerhead ribozyme, DI genome sequence, hepatitis D virus ribozyme, T7 termination sequence, and XbaI restriction site. These cassettes were then cloned via BamHI/XbaI restriction cloning into a pUC57 backbone (GenScript). Individual DI plasmids, in conjunction with Pol-II-based plasmids expressing T7 polymerase and NiV-M nucleoprotein (N), phosphoprotein (P), and RNA-dependent RNA-polymerase (L) protein, were transfected into BSR-T7/5 cells in a 15:15:6:2:2 ratio, respectively, using LT-1 transfection reagent (Mirius). At 2 days post transfection (dpt), BSR-T7/5 cells were overlayed with an equal number of Vero cells and infected with rNiV-M/ZsG at a multiplicity of infection (MOI) of 0.01 (based on Vero cell number only). The supernatant was removed 7 dpt, clarified by low-speed centrifugation (1500 rpm, 10 minutes), and frozen until use.

DIP Inhibition Assay

To create DIP stocks depleted of producer virus (rNiV-M/ZsG), termed active DIPs, stocks were treated with 100 mJ/cm^2 of ultraviolet (UV) radiation (CX-2000 Crosslinker; UVP) in a 6-well plate (1 mL per well). To create DIP stocks depleted of both the producer virus and any DI genomes (termed inactive DIPs), stocks were treated with 10 × 240 mJ/cm^2 of UV radiation. For the inhibition assay, Vero cells were first seeded in a 24-well plate at 5 × 10^4 cells per well in 500 μL medium. For each DIP, 2 × 10^3 $TCID_{50}$ of virus (diluted in DMEM to 1 mL) was added to 1 mL active or inactive DIP stock, and 500 μL of the mixture was then used to infect each well (final MOI of 0.01). At 2 days postinfection (dpi), supernatant was collected and NiV-M titers were determined by $TCID_{50}$ in Vero cells [24]. Fold reduction in NiV titers for each DIP was calculated by dividing titers from the inactive DIP-treated cell with the titers from the active DIP-treated cells.

Digital Droplet Quantitative Reverse-Transcription Polymerase Chain Reaction

A 20× mix of Di-specific or NiV-specific primers and probes (18 μM each primer and 5 μM probe) were used in conjunction with 1-Step RT-ddPCR Advanced Kit for Probes and Droplet Generation Oil for Probes (both from Bio-Rad). Duplex quantitative reverse-transcription polymerase chain reaction (qRT-PCR) reactions were set up and run as per manufacturers' conditions, with droplets generated using QX200 Droplet Generator (Bio-Rad). Results were analyzed using QX200 Droplet Digital PCR System, and quantification data were generated using QuantaSoft Software (both from Bio-Rad).

Data Analysis and Graphics

All graphs were created in GraphPad Prism (version 8.2.0). All fluorescent microscopy images were taken using the EVOS cell imaging system (Thermo Fisher Scientific). DIP production schematic was created with BioRender.com. For DIP inhibition curves, titers were used to fit a 4-parameter equation to semilog plots of the ratio-inhibition data. From this, the DIP:NiV genome ratios causing 1000-fold reduction in NiV titers were interpolated. Significance was calculated using a 1-sample *t* test.

RESULTS

High Multiplicity of Infection Passaging of NiV Results in the Production of Multiple Defective Viral Genome Species

To create naturally occurring NiV DI genomes, several strains of the virus were repeatedly passaged with minimal dilution per passage, a process known to increase frequency of DI genome generation [22, 27, 28]. Vero cells were initially infected at an MOI of >1 with NiV-M, NiV-B, rNiV-M, rNiV-M/ZsG, or 2 mutant rNiVs unable to produce full-length C protein, rNiV-M C-, and rNiV-M D156 (Figure 1A). In paramyxoviruses, the C protein is a polymerase cofactor important in maintaining fidelity, and its removal has been shown to increase copyback DI frequency in measles virus (MeV) [29], Sendai virus (SeV) [30], and human parainfluenza virus 1 (hPIV1) [31]. At 2–4 dpi, when extensive CPE became apparent, the supernatant was removed and clarified by low-speed centrifugation to pellet cells and debris, and 50% of it was transferred to fresh Vero cells. This process was continued for 10 passages using NiV-M, NiV-B, rNiV-M, and rNiV-M/ZsG strains. For rNiV-M C- and rNiV-M D156 strains, the experiment was halted after 5 passages due to the substantial reductions in titers observed.

In general, a reduction in viral titers was observed with increasing passage number, with the greatest drop seen between passage 3 and passage 5 for all strains tested (Figure 1B). For all viruses, increasing passage number was associated with delayed appearance of NiV-mediated CPE. Likewise, the most concentrated dilutions of cell culture supernatant did not fully clear Vero cell monolayers via CPE during titration experiments to determine $TCID_{50}$. This effect, which diluted out before NiV diluted out, indicated the presence of DIPs in the supernatant, and was more pronounced in the rNiV-M C- and rNiV-M D156 experiments (Figure 1C).

RNA from clarified cell culture supernatants was analyzed to detect DI genomes capable of being packaged into NiV-like virions, with samples from passages 3, 4, 5, and 10 for all viruses sequenced and analyzed. The Illumina sequencing dataset was analyzed for presence of break and reinitiation points indicative of DI genomes and allowed extrapolation of the entire deletion or copyback nucleotide sequence. NGS and subsequent bioinformatic analysis consistently identified multiple DI species present in the viral RNA for each tested passage, although a single species generally made up 90%–99% of all DI species detected. For all viral passage experiments, the principal DI species found at the earliest tested passage was also the principal species seen at all later passages, indicating that whatever species prevailed initially continued to predominate. These datasets were further refined to include only DI genomes obeying the paramyxovirus “rule of six”, and those with >10 independent detections of the same break and reinitiation point in the same RNA sample. In total, 25 naturally occurring DI genomes were characterized (Table 1). To supplement these, several in silico-designed deletion DIs were additionally generated: DI-19 to DI-22, containing equal proportions of both leader and trailer sequences; and DI-23 to DI-25, with varying proportions of leader and trailer sequences. Furthermore, deletion DI genomes based on minigenome segments capable of expressing the fluorescent proteins dTomato

(DI-dTom) and blue fluorescent protein (DI-BFP), and the luminescent protein *Gaussia* luciferase (DI-gLuc), were also included (Figure 2).

Artificial DIP Can Be Generated Using Infectious NiV as a Producer Virus

Of the 25 naturally occurring DI genomes characterized, 9 were selected for DIP production. Selection was based on both nucleotide length (<2 kilobases total preferred) and internal structure (DI genomes with varied break and reinitiation points were chosen). All in silico-designed DI genomes were also included. To produce artificial DIPs, a modified version of the NiV reverse genetics system was used [32], with the DI-expressing plasmid transfected into BSR-T7/5 cells along with support plasmids capable of expressing viral proteins necessary for NiV replication: N, L, and P (Figure 3A). At 2 dpt, these cells were overlayed with Vero cells, and then infected with rNiV-M/ZsG (MOI of 0.01), which acted as a producer virus. The presence of a producer virus was required to supply the nascent DI RNPs with all required proteins for packaging, assembly, and release of the DIPs. Overlaying with Vero cells was incorporated into the production method because they are much more permissive to NiV infection and spread than BSR-T7/5 cells. At 5 dpi (7 dpt), DIPs were harvested by collecting the cell culture supernatant (clarified by low-speed centrifugation). However, DIP stocks at this stage still contained the producer rNiV-M/ZsG and remained infectious. Therefore, taking advantage of the large difference in genome size between rNiV-M/ZsG and the DI, a precise dose of UV radiation was used to remove the infectious component but leave the DIP component of the stock relatively unaffected. A range of UV radiation doses was evaluated using only rNiV-ZsG to determine the minimal amount required to completely remove producer (full length) virus infectivity (Figure 3B). A dose of 100 mJ/cm^2 UV was used to ensure complete inactivation of the producer virus but leave DI genomes intact (stocks termed active DIPs). A dose of 10 × 240 mJ/cm^2 UV was used to ensure complete inactivation of both the producer virus and DI genomes (stocks termed inactive DIPs).

To ensure that this procedure produced fully functional, entry-competent, replication-deficient DIPs, we examined expression of the dTom reporter protein from DI-dTom (Figure 3C). Fluorescent signal from both ZsG (producer virus) and dTom (DI-dTom) was detectable in untreated samples at passage 1 (P1) and was retained in passage 2 (P2). For active DIPs with no additional rNiV-M/ZsG, no ZsG or dTom was detected at either P1 or P2, demonstrating that DIPs are inactive in the absence of authentic virus. Detection of dTom in P1 cells treated with active DIP and rNiV-M/ZsG underscored that DIP genomes remain unaffected by the 100 mJ/cm^2 UV dose. The retention of dTom fluorescence in P2 cells further demonstrated that the DI genome was packaged correctly and able to enter cells. In cells treated with inactive DIPs with no additional rNiV-M/ZsG, no ZsG or dTom signal was detected, and adding rNiV/ZsG did not restore the dTom signal, indicating complete destruction of the DI genome.

Artificial DIP Are Capable of Inhibiting NiV

In vitro DIP inhibition was assessed by determining endpoint titers of rNiV-M virus when mixed with either active (treated with 100 mJ/cm^2 UV) or inactive (treated with 10 × 240 mJ/cm^2 UV) DIPs. A mixture of DIP and rNiV-M (MOI of 0.01) was used to infect

Vero cells, and after 48 hours cell culture supernatants were removed and viral titers were determined. Inhibition was determined by calculating relative fold reduction in rNiV-M titer between the active and inactive DIPs. All but 1 DIP (DI-09) containing naturally occurring DI genomes demonstrated at least a relative 100-fold reduction in titers, with DI-10, DI-14, DI-15, DI-16, and DI-35 resulting in a >1000-fold reduction (Figure 4A). The 3 DIPs containing minigenome segment genomes demonstrated comparable ~100-fold levels of inhibition. None of the 7 DIPs containing in silico-designed DI genomes significantly inhibited rNiV-M.

We then selected the 9 best performing DIP candidates and determined the DIP concentration in each stock using specific qRT-PCR assays designed to produce an amplicon spanning the break and reinitiation point of each DI genome. This ensured exponential amplification of only that specific DI genome over that of a different DI genome or the producer virus. Using digital droplet qRT-PCR to quantify DIP concentrations, 3 independent DIP production assays consistently generated between 5×10^7 and 5×10^8 DI genome copies/mL (Figure 4B). These DIP titers were similar to the titers of NiV virus (determined again by qRT-PCR) in control samples (cells originally transfected with empty plasmid in place of DI-expressing plasmid), which generated approximately 1×10^8 NiV genomes copies/mL. The inhibition experiment was repeated with these DIPs, with stocks normalized to give a DI:NiV genome ratio of 5000:1, using both prototypic strains of NiV-M and NiV-B alongside rNiV-M. All DIPs inhibited rNiV-M and NiV-M more strongly than they did NiV-B (Figure 4C). The minor disparity in DIP efficacy between the 2 strains is likely a result of the small number of nucleotide differences in the 5′ and 3′ terminal regions, causing suboptimal replication of DIs by the NiV-B viral proteins, and therefore reduced inhibitory effects.

Finally, experiments were performed to both assess whether the RNA component of the DIP was necessary for inhibition and to rule out any nonspecific, non-DI-mediated NiV inhibition. NiV dose-response curves were performed using the best overall performing DIPs: DI-07, DI-10, DI-14, DI-15, and DI-35. Mixtures containing a range of DI:rNiV-M genome ratios from 20 000:1 to 78:1, both for active and inactive DIPs, were used to infect Vero cells, and titers were determined 48 hours postinfection (Figure 4D). More important, for the inactive DIPs, no significant reduction in rNiV-M titers was observed at any ratio of DI:rNiV genomes, indicating that inhibition was mediated, at least in part, by intact DI genomes. Significant reduction in rNiV-M titers was observed when active DIPs were used at the highest DI:rNiV genomes ratios, with inhibition weakening as the ratio decreased. The ratio of DI:rNiV genome required for a 1000-fold reduction was calculated for each DIP to be as follows: DI-07 = 2510:1; DI-10 = 4483:1; DI-14 = 4853:1; DI-15 = 1702:1; and DI-35 = 11 653:1.

DISCUSSION

Artificially generated DIPs represent a novel approach to antiviral development, hijacking a naturally occurring process that constrains viral replication and utilizing it as a therapy. Although the concept of using DIPs as antivirals is not a new one [28, 33-35], the recent development of more advanced techniques, allowing the cloning and generation of specific

DI species, has increased the interest in their antiviral potential. Several studies, both in vitro and in vivo, have described paramyxovirus species DIs and their biological functions, including interference of authentic viral replication (hPIV3 [36], MeV [37], and SeV [38]), interferon (IFN)-induction (hPIV1 [31], parainfluenza virus 5 (PIV5) [39], MeV [40], and SeV [41]), and viral persistence (MeV [42], mumps virus [43], and SeV [44]). In this study, we have characterized a large pool of naturally occurring NiV DI genomes, and we subsequently generated DIPs using reverse genetics based on these and other in silico-designed DI genomes.

These data demonstrate that a large and diverse population of naturally occurring NiV DI genomes generated by high MOI passaging can be individually investigated and characterized using NGS alone. This approach revealed a strong preference towards production of NiV copyback DI genome species compared with deletion DIs. This has similarly been reported for other negative-sense, single-stranded RNA viruses including Ebola virus [45] and PIV5 [39], and it is likely due to the difference in relative strength of genome replication initiation between trailer (stronger) and leader (weaker) (reviewed in [46]). However, although the occurrence of copybacks may be more frequent, the inhibitory activity seems comparable to deletions; the 1 natural deletion we incorporated into the inhibition assays reduced NiV titers to the same degree as the natural copyback DIs.

In general, shorter DI genomes inhibited NiV more robustly than longer ones, and naturally occurring DI genomes were superior to in silico-designed DI genomes in virus interference assays. The increased activity of shorter DIs is likely attributed to increased replication efficiency, resulting in a greater intracellular concentration compared with longer DIs. However, explanations for the increased inhibition observed for naturally occurring DIs over in silico-designed DI genomes remain unclear. One explanation may be that, because we still do not fully understand many aspects of DI generation, these in silico-designed DI genomes may be missing as yet unidentified factors, such as cisacting nucleotide motifs necessary for replication and packaging, and are therefore unable to efficiently compete with standard virus.

Numerous studies have reported the highly immunogenic properties of DI genomes, where, in particular, the structural characteristics of copybacks (dsRNA blunt-end hairpin with a 5'-triphosphate extremity) are sensed by members of the RIG-I-like receptor family and induce type-I IFN responses [47-49]. We were able to show that DI-induced inhibition of NiV is, in part, independent of this response by demonstrating inhibition in Vero cells that are unable to produce type-1 IFN. This underscores the importance of the nucleic acid component of the DIP, and it suggests that inhibition may be a result of direct competition between DI genomes and authentic viral genomes for the viral protein pool and potentially some host cell factors. However, in addition to direct effects of the DI, eliciting an immune response to DIP therapy may also be beneficial in a treatment regimen, by synergistically utilizing both direct and indirect mechanisms of interference to boost therapeutic efficacy.

CONCLUSIONS

The therapeutic application of DIPs may offer several potential benefits over the more traditional antiviral approaches: they are transmissible in the presence of authentic virus and therefore able to disseminate alongside virus to target the same infected cells and tissues; unlike vaccine-mediated immunity via priming of the adaptive and innate immune pathways, DIP-mediated protection is effective immediately, and DIPs are non-replicating and transcriptionally inert in the absence of authentic virus, thus reducing potential side effects. We have shown that artificially generated NiV DIPs are capable of reducing viral titers by over 1000-fold in vitro. There is evidence that artificially generated therapeutic DIPs can protect against disease in vivo, as was demonstrated in ferrets challenged with lethal doses of IAV [12-15]. Additional studies demonstrating efficacy in small animal models of NiV would further support develop of DIP treatment platforms. In summary, the benefits offered by DIP therapy, along with in vitro therapeutic efficacy of DIs against NiV demonstrated here, support Nipah DI therapy as a promising approach to combat this high-threat pathogen.

Supplementary Material

Refer to Web version on PubMed Central for supplementary material.

Acknowledgments.

We thank Tatyana Klimova for assistance with editing the manuscript.

Financial support.

This work was partially funded by an appointment to the Research Participation Program at the Centers for Disease Control and Prevention (CDC) administered by the Oak Ridge Institute for Science and Education through an interagency agreement between the US Department of Energy and CDC (to S. R. W.) and the DARPA INTERfering and Co-Evolving Prevention and Therapy (INTERCEPT) program (DARPA-BAA-16–35) and by CDC Emerging Infectious Disease Research Core Funds.

References

1. von Magnus P. Propagation of the PR8 strain of influenza A virus in chick embryos. II. The formation of incomplete virus following inoculation of large doses of seed virus. Acta Pathol Microbiol Scand 1951; 28:278–93. [PubMed: 14856732]
2. Huang AS, Baltimore D. Defective viral particles and viral disease processes. Nature 1970; 226:325–7. [PubMed: 5439728]
3. Vignuzzi M, López CB. Defective viral genomes are key drivers of the virus-host interaction. Nat Microbiol 2019; 4:1075–87. [PubMed: 31160826]
4. Vasilijevic J, Zamarreño N, Oliveros JC, et al. Reduced accumulation of defective viral genomes contributes to severe outcome in influenza virus infected patients. PLoS Pathog 2017; 13:e1006650. [PubMed: 29023600]
5. Barrett AD, Guest AR, Mackenzie A, Dimmock NJ. Protection of mice infected with a lethal dose of semliki forest virus by defective interfering virus: modulation of virus multiplication. J Gen Virol 1984; 65:1909–20. [PubMed: 6094709]
6. Holland JJ, Doyle M. Attempts to detect homologous autointerference in vivo with influenza virus and vesicular stomatitis virus. Infect Immun 1973; 7:526–31. [PubMed: 4357601]
7. Martínez-Gil L, Goff PH, Hai R, García-Sastre A, Shaw ML, Palese P. A Sendai virus-derived RNA agonist of RIG-I as a virus vaccine adjuvant. J Virol 2013; 87:1290–300. [PubMed: 23175362]

8. Bellocq C, Mottet G, Roux L. Wide occurrence of measles virus subgenomic RNAs in attenuated live-virus vaccines. Biologicals 1990: 18:337–43. [PubMed: 2285505]
9. McLaren LC, Holland JJ. Defective interfering particles from poliovirus vaccine and vaccine reference strains. Virology 1974; 60:579–83. [PubMed: 4367496]
10. Dimmock NJ, Rainsford EW, Scott PD, Marriott AC. Influenza virus protecting RNA: an effective prophylactic and therapeutic antiviral. J Virol 2008; 82:8570–8. [PubMed: 18579602]
11. Zhao H, To KK, Chu H, et al. Dual-functional peptide with defective interfering genes effectively protects mice against avian and seasonal influenza. Nat Commun 2018; 9:2358. [PubMed: 29907765]
12. Dimmock NJ, Dove BK, Scott PD, et al. Cloned defective interfering influenza virus protects ferrets from pandemic 2009 influenza A virus and allows protective immunity to be established. PLoS One 2012; 7:e49394. [PubMed: 23251341]
13. Dimmock NJ, Dove BK, Meng B, et al. Comparison of the protection of ferrets against pandemic 2009 influenza A virus (H1N1) by 244 DI influenza virus and oseltamivir. Antiviral Res 2012; 96:376–85. [PubMed: 23041142]
14. Scott PD, Meng B, Marriott AC, Easton AJ, Dimmock NJ. Defective interfering influenza virus confers only short-lived protection against influenza virus disease: evidence for a role for adaptive immunity in DI virus-mediated protection in vivo. Vaccine 2011; 29:6584–91. [PubMed: 21762748]
15. Scott PD, Meng B, Marriott AC, Easton AJ, Dimmock NJ. Defective interfering influenza A virus protects in vivo against disease caused by a heterologous influenza B virus. J Gen Virol 2011; 92:2122–32. [PubMed: 21632569]
16. Chua KB, Bellini WJ, Rota PA, et al. Nipah virus: a recently emergent deadly paramyxovirus. Science 2000; 288:1432–5. [PubMed: 10827955]
17. Hsu VP, Hossain MJ, Parashar UD, et al. Nipah virus encephalitis reemergence, Bangladesh. Emerg Infect Dis 2004; 10:2082–7. [PubMed: 15663842]
18. Chadha MS, Comer JA, Lowe L, et al. Nipah virus-associated encephalitis outbreak, Siliguri, India. Emerg Infect Dis 2006; 12:235–40. [PubMed: 16494748]
19. Luby SP. The pandemic potential of Nipah virus. Antiviral Res 2013; 100:38–43. [PubMed: 23911335]
20. Lo MK, Rota PA. The emergence of Nipah virus, a highly pathogenic paramyxovirus. J Clin Virol 2008; 43:396–400. [PubMed: 18835214]
21. Sharma V, Kaushik S, Kumar R, Yadav JP, Kaushik S. Emerging trends of Nipah virus: a review. Rev Med Virol 2019; 29:e2010. [PubMed: 30251294]
22. Manzoni TB, López CB. Defective (interfering) viral genomes re-explored: impact on antiviral immunity and virus persistence. Future Virol 2018; 13:493–503. [PubMed: 30245734]
23. Lo MK, Nichol ST, Spiropoulou CF. Evaluation of luciferase and GFP-expressing Nipah viruses for rapid quantitative antiviral screening. Antiviral Res 2014; 106:53–60. [PubMed: 24680955]
24. Reed LJ, Muench H. A simple method for estimating fifty percent endpoints. Am J Epidemiol 1938; 27:493–497.
25. Whitmer SLM, Ladner JT, Wiley MR, et al. Active Ebola virus replication and heterogeneous evolutionary rates in EVD survivors. Cell Rep 2018; 22:1159–68. [PubMed: 29386105]
26. Ladner J. chimeric_reads. Available at: https://github.com/jtladner/Scripts/tree/master/chimeric_reads. Accessed .
27. Magnus P von. Incomplete forms of influenza virus. Adv Virus Res 1954; 2:59–79. [PubMed: 13228257]
28. Dimmock NJ, Easton AJ. Defective interfering influenza virus RNAs: time to reevaluate their clinical potential as broad-spectrum antivirals? J Virol 2014; 88:5217–27. [PubMed: 24574404]
29. Pfaller CK, Radeke MJ, Cattaneo R, Samuel CE. Measles virus C protein impairs production of defective copyback double-stranded viral RNA and activation of protein kinase R. J Virol 2014; 88:456–68. [PubMed: 24155404]

30. Sánchez-Aparicio MT, Garcin D, Rice CM, Kolakofsky D, García-Sastre A, Baum A. Loss of Sendai virus C protein leads to accumulation of RIG-I immunostimulatory defective interfering RNA. J Gen Virol 2017; 98:1282–93. [PubMed: 28631605]
31. Boonyaratanakornkit J, Bartlett E, Schomacker H, et al. The C proteins of human parainfluenza virus type 1 limit double-stranded RNA accumulation that would otherwise trigger activation of MDA5 and protein kinase R. J Virol 2011; 85:1495–506. [PubMed: 21123378]
32. Lo MK, Peeples ME, Bellini WJ, Nichol ST, Rota PA, Spiropoulou CF. Distinct and overlapping roles of Nipah virus P gene products in modulating the human endothelial cell antiviral response. PLoS One 2012; 7:e47790. [PubMed: 23094089]
33. Barrett ADT, Dimmock NJ. Modulation of a systemic Semliki Forest virus infection in mice by defective interfering virus. J Gen Virol 1984; 65:1827–31. [PubMed: 6092526]
34. Jones CL, Holland JJ. Requirements for DI particle prophylaxis against vesicular stomatitis virus infection in vivo. J Gen Virol 1980; 49:215–20. [PubMed: 6252288]
35. Dimmock NJ, Easton AJ. Cloned defective interfering influenza RNA and a possible pan-specific treatment of respiratory virus diseases. Viruses 2015; 7:3768–88. [PubMed: 26184282]
36. Murphy DG, Dimock K, Yong Kang C. Defective interfering particles of human parainfluenza virus 3. Virology 1987; 158:439–43. [PubMed: 3035791]
37. Calain P, Roux L. Generation of measles virus defective interfering particles and their presence in a preparation of attenuated live-virus vaccine. J Virol 1988; 62:2859–66. [PubMed: 3392771]
38. Portner A, Kingsbury DW. Identification of transcriptive and replicative intermediates in Sendai virus-infected cells. Virology 1972; 47:711–25. [PubMed: 4335074]
39. Killip MJ, Young DF, Gatherer D, et al. Deep sequencing analysis of defective genomes of parainfluenza virus 5 and their role in interferon induction. J Virol 2013; 87:4798–807. [PubMed: 23449801]
40. Shivakoti R, Siwek M, Hauer D, Schultz KL, Griffin DE. Induction of dendritic cell production of type i and type III interferons by wild-type and vaccine strains of measles virus: role of defective interfering RNAs. J Virol 2013; 87:7816–27. [PubMed: 23678166]
41. Yount JS, Gitlin L, Moran TM, López CB. MDA5 participates in the detection of paramyxovirus infection and is essential for the early activation of dendritic cells in response to Sendai virus defective interfering particles. J Immunol 2008; 180:4910–8. [PubMed: 18354215]
42. Sidhu MS, Crowley J, Lowenthal A, et al. Defective measles virus in human subacute sclerosing panencephalitis brain. Virology 1994; 202:631–41. [PubMed: 8030228]
43. Andzhaparidze OG, Boriskin YS, Bogomolova NN, Drynov ID. Mumps virus-persistently infected cell cultures release defective interfering virus particles. J Gen Virol 1982; 63:499–503. [PubMed: 7153766]
44. Xu J, Sun Y, Li Y, et al. Replication defective viral genomes exploit a cellular pro-survival mechanism to establish paramyxovirus persistence. Nat Commun 2017; 8:799. [PubMed: 28986577]
45. Calain P, Monroe MC, Nichol ST. Ebola virus defective interfering particles and persistent infection. Virology 1999; 262:114–28. [PubMed: 10489346]
46. Lamb RA, Parks GD. Paramyxoviridae: the viruses and their replication. In Fields BN, Knipe DN, Howley PM, Eds. Fields virology. Lippincott, Williams, and Wilkins, 2007: 1449–1496.
47. Baum A, Sachidanandam R, Garcia-Sastre A, García-Sastre A. Preference of RIG-I for short viral RNA molecules in infected cells revealed by next-generation sequencing. Proc Natl Acad Sci U S A 2011; 108:3092.
48. Mura M, Combredet C, Najburg V, David RY, Tangy F, Komarova AV. Nonencapsidated 5’ copy-back defective interfering genomes produced by recombinant measles viruses are recognized by RIG-I and LGP2 but not MDA5. J Virol 2017; 91:643–60.
49. Poole E, He B, Lamb RA, Randall RE, Goodbourn S. The V proteins of simian virus 5 and other paramyxoviruses inhibit induction of interferon-β. Virology 2002; 303:33–46. [PubMed: 12482656]

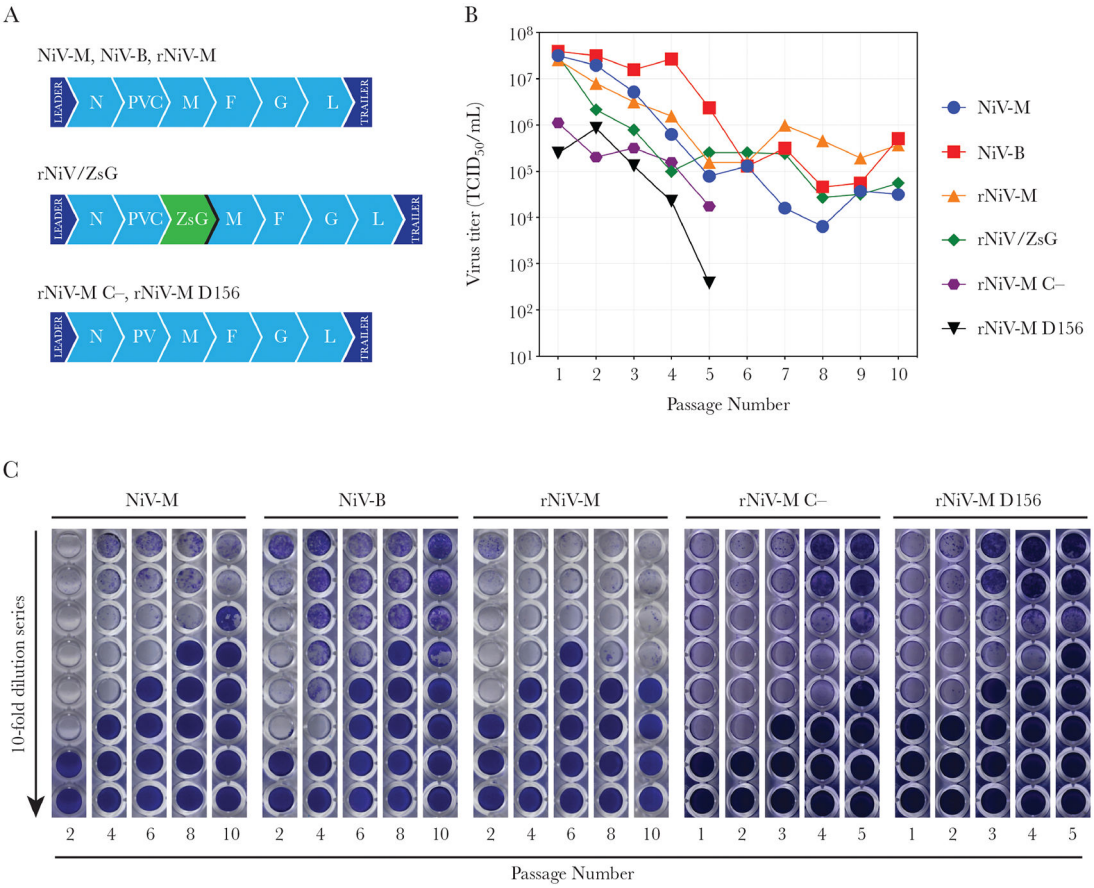

Figure 1.

Generation and detection of naturally occurring Nipah virus (NiV) defective viral genomes. (*A*) Genome schematics of the NiV strains used during high multiplicity of infection passaging. (*B*) Titers of viruses used at each passage. (*C*) Representative images of the Vero cell monolayers from 50% tissue culture infective dose ($TCID_{50}$) determination plates for NiV-M, NiV-B, rNiV-M, rNiV-M C-, and rNiV-M D156 at select passage numbers. Plates were fixed and stained with crystal violet (0.1%). F, fusion protein; G, glycoprotein; L, ribonucleic acid (RNA)-dependent RNA polymerase; M, matrix protein; NiV-B, NiV Bangladesh strain; NiV-M, NiV Malaysia strain; rNiV-M, NiV Malaysia; rNiV-M C- and rNiV-M D156, recombinant NiV Malaysia with different mutations introduced to stop expression of the C protein; rNiV-M/ZsG, recombinant NiV Malaysia expressing ZsGreen1 fluorescent protein; N, nucleoprotein; PVC, P, C, and V protein open reading frame.

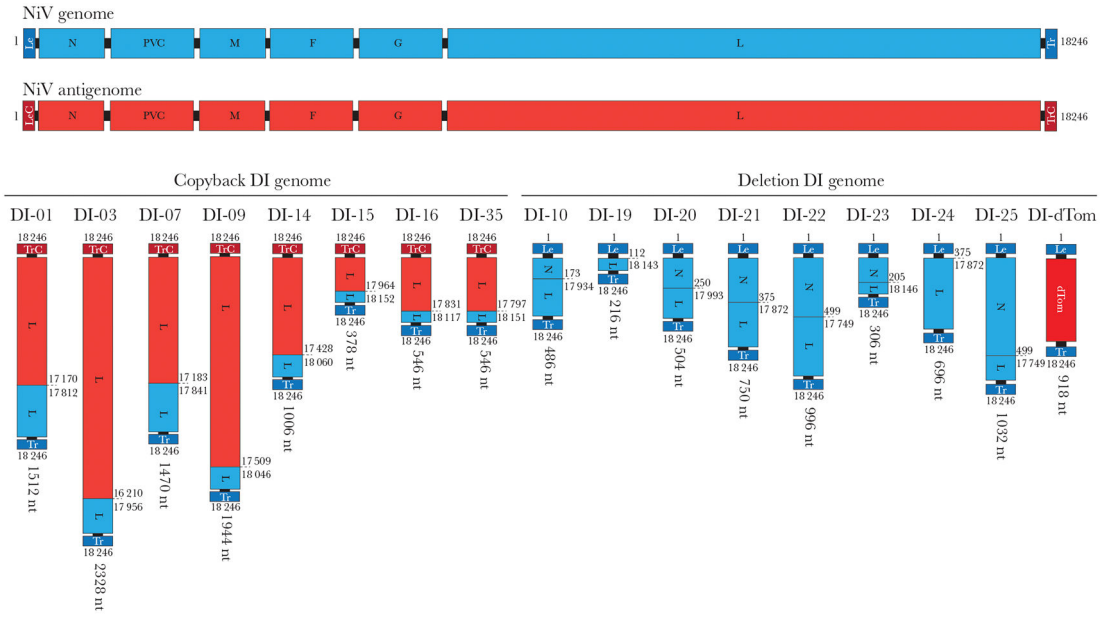

Figure 2.

Structures of the NiV defective interfering (DI) genomes. The structures of the 8 naturally occurring (7 trailer copyback and 1 deletion) and 8 in silico-designed (7 deletion and 1 minigenome) DI genomes. Represented in the full NiV genome in genomic (blue) and antigenomic (red) sense. Nucleotide position of break and reinitiation points are given based on antigenomic sense NiV-M (GenBank accession no. AF212302). Total length of DI genome is given in nucleotides (nt). F, fusion protein; G, glycoprotein; L, ribonucleic acid (RNA)-dependent-RNA-polymerase; Le, leader sequence; LeC, leader complementary sequence; M, matrix protein; N, nucleoprotein; PVC, P, C, and V protein open reading frames; Tr, trailer sequence; TrC, trailer complementary sequence.

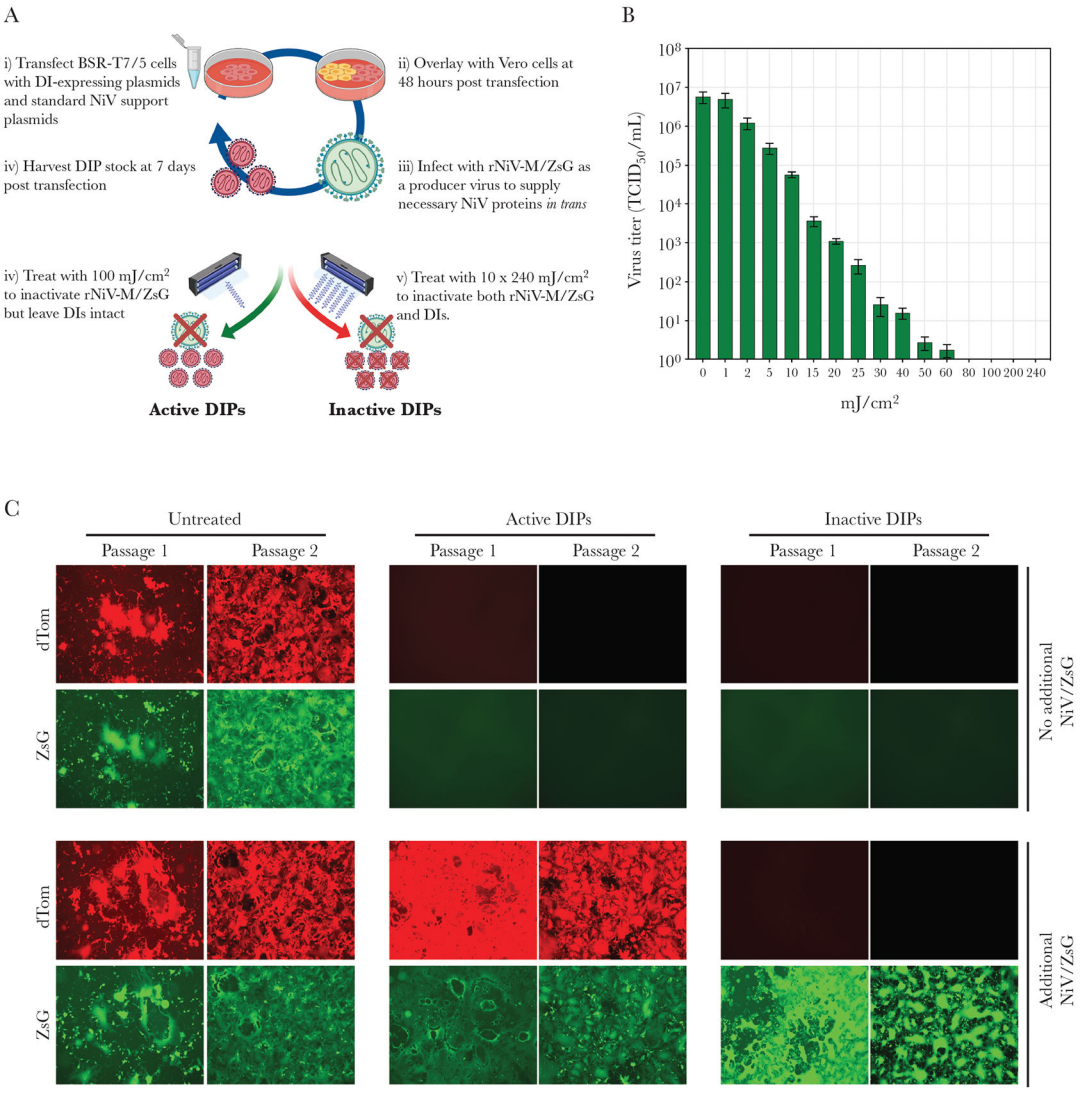

Figure 3.

NiV defective interfering particles (DIPs) can be artificially generated using producer virus. (*A*) Production of artificial NiV DIPs using rNiV-ZsG as a producer virus, and selective inactivation using ultraviolet (UV) radiation of either rNiV-M/ZsG only (100 mJ/cm^2 of UV) or both rNiV-M/ZsG and DIPs (10 × 240 mJ/cm^2 of UV) to produce active and inactive DIPs, respectively. (*B*) Reduction in infectious rNiV-M/ZsG titer using UV radiation to inactivate virus. (*C*) Validation of production and inactivation assay. Passage 1 images represent either dTom or ZsG fluorescence detected in Vero cell monolayers 48 hours post infection (hpi) after treatment with 1 mL untreated DI-dTom, active DI-dTom, or inactive DI-dTom. Passage 2 images represent either dTom or ZsG fluorescence detected in Vero cell monolayers 48 hpi after addition of 1 mL cell culture supernatant from passage 1. Only passage 1 involved UV treatments and addition of supplementary rNiV-M/ZsG.

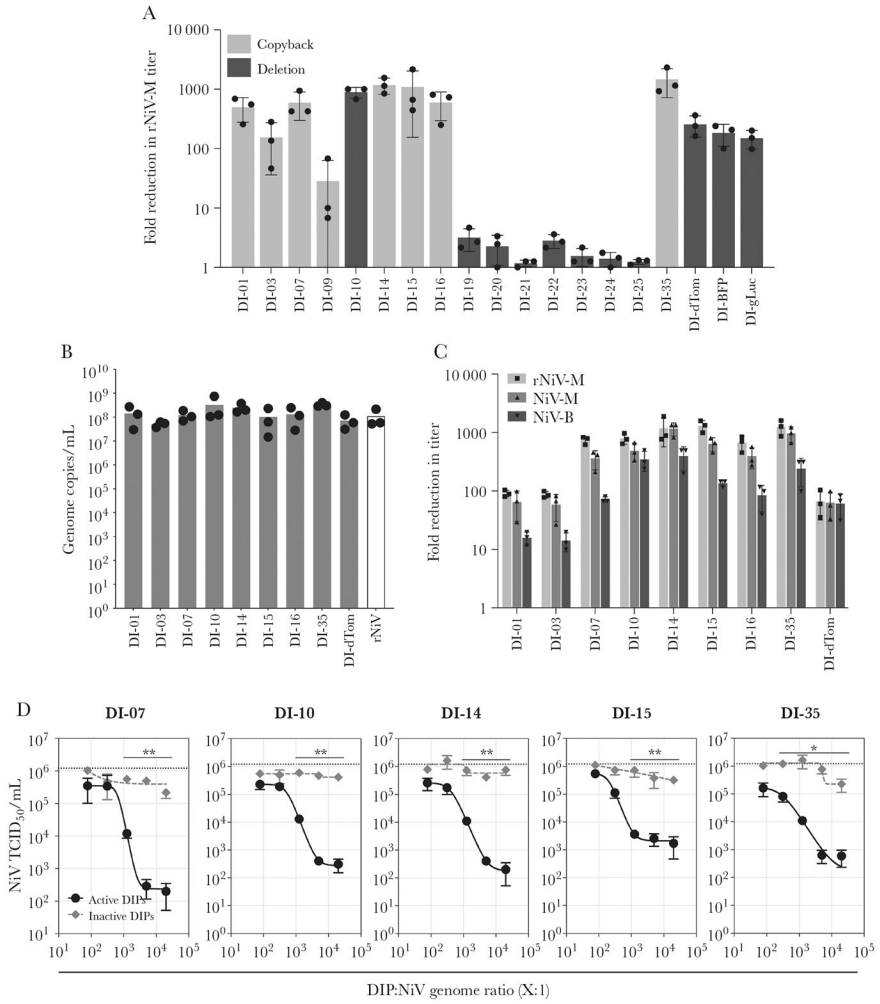

Figure 4.

Inhibition of NiV by treatment with artificial DIPs. (*A*) Inhibition of rNiV-M titers in Vero cells after treatment with DIPs. Vero cells were treated with either active or inactive DIPs mixed with 0.01 multiplicity of infection (MOI) rNiV-M, and rNiV-M titers were determined 48 hpi. Represented is fold reduction in titer (fold difference in titer between cells treated with active DIP and cells treated with inactive DIPs). Represented is a scatter plot, with bars showing data performed in triplicate; lines represent mean and standard deviation. (*B*) Quantification of DIP concentrations (DIP genome copies/mL) using DIP-specific digital droplet quantitative reverse-transcription polymerase chain reaction (qRT-PCR). The rNiV represents rNiV-M genome concentrations in control (no DIP) production assay using a NiV-specific dd qRT-PCR. Represented is a scatter plot with bars showing data from 3 independent DIP production assays. (*C*) Inhibition of rNiV-M (■), NiV-M (▲), and NiV-B (▼) titers in Vero cells after treatment with DIPs. Vero cells were treated with either active or inactive DIPs mixed with rNiV-M (DIP:NiV genome ratio normalized to 5000:1; cells infected at MOI of 0.01), with endpoint titers determined 48 hpi. Represented is fold reduction in titer (fold difference in titers between cells treated with active DIP and cells treated with inactive DIPs). Represented is a scatter pot with bars showing data performed in

triplicate; lines represent mean and standard deviation. (*D*) Dose-response curves for DI-07, DI-10, DI-14, DI-15, and DI-35. Normalized active (●) and inactive(◆) DIP stocks were mixed with rNiV-M at genome ratios of 20 000:1, 5000:1, 1250:1, 313:1, and 78:1 and used to infect Vero cells (final MOI of 0.01); 48 hpi, endpoint rNiV-M titers were determined. Dotted line represents rNiV-M titers in untreated control cells. Data represent assay run in triplicate; bars represent mean and standard deviation. Statistical differences calculated by *t* test on mean titers between active and inactive treated samples: *, $P < .05$; **, $P < .01$).

Table 1.

Break and Reinitiation Points on NiV DI Genomes[a]

DI Genome	Genome Breakpoint (nt)	Genome Reinitiation Point (nt)	Length (nt)	Overlap	DI Genome Classification	DI Genome Type	Virus Used to Generate DI Genome
DI-01	17170	17812	1512	0	Trailer copyback	Natural	rNiV-M C-
DI-03	16210	17953	2328	3	Trailer copyback	Natural	rNiV-M C-
DI-04	14776	16773	4944	1	Trailer copyback	Natural	rNiV-M C-
DI-05	16177	17827	2490	0	Trailer copyback	Natural	rNiV-M C-
DI-06	12657	17267	6570	0	Trailer copyback	Natural	rNiV-M
DI-07	17183	17840	1470	1	Trailer copyback	Natural	rNiV-M
DI-08	15715	15919	4860	0	Trailer copyback	Natural	rNiV-M
DI-09	16503	18046	1944	1	Trailer copyback	Natural	rNiV-M
DI-10	173	17932	486	2	Deletion	Natural	rNiV-M C-
DI-14	17428	18060	1014	0	Trailer copyback	Natural	rNiV-M C-
DI-15	17964	18152	378	0	Trailer copyback	Natural	rNiV-M D156
DI-16	17831	18112	546	5	Trailer copyback	Natural	rNiV-M D156
DI-18	16064	17716	2712	2	Trailer copyback	Natural	rNiV-M D156
DI-19	112	18143	216	0	Deletion	In silico	n/a
DI-20	250	17993	504	0	Deletion	In silico	n/a
DI-21	375	17872	750	0	Deletion	In silico	n/a
DI-22	499	17749	996	0	Deletion	In silico	n/a
DI-23	205	18147	306	0	Deletion	In silico	n/a
DI-24	98	17649	696	0	Deletion	In silico	n/a
DI-25	825	18040	1032	0	Deletion	In silico	n/a
DI-27	17289	17674	1530	1	Trailer copyback	Natural	rNiV-M D156
DI-28	16250	17050	3192	2	Trailer copyback	Natural	rNiV-M D156
DI-29	17633	17756	1104	1	Trailer copyback	Natural	rNiV-M D156
DI-30	14076	16554	5862	2	Trailer copyback	Natural	rNiV-M D156
DI-31	17511	17723	1260	0	Trailer copyback	Natural	rNiV-M D156
DI-32	16216	18123	2154	1	Trailer copyback	Natural	rNiV-M D156
DI-33	17706	17840	948	0	Trailer copyback	Natural	rNiV-M D156
DI-34	15218	15820	5454	2	Trailer copyback	Natural	rNiV-M/ZsG

DI Genome	Genome Breakpoint (nt)	Genome Reinitiation Point (nt)	Length (nt)	Overlap	DI Genome Classification	DI Genome Type	Virus Used to Generate DI Genome
DI-35	17797	18150	546	1	Trailer copyback	Natural	rNiV-M/ZsG
DI-36	15676	16971	3846	1	Trailer copyback	Natural	NiV-B
DI-38	807	18104	950	0	Deletion	Natural	rNiV-M D156
DI-dTom	112	18147	918	0	Minigenome	In silico	n/a
DI-BFP	112	18147	918	0	Minigenome	In silico	n/a
DI-gLuc	112	18147	918	0	Minigenome	In silico	n/a

Abbreviations: BFP, blue fluorescent protein; DI, defective interfering; dTom, dTomato; gLuc, *Gaussia* luciferase; n/a, not applicable; NiV, Nipah virus; nt, nucleotide.

[a]Nucleotide position based on antigenomic sense of NiV-M (GenBank accession no. AF212302). Overlap signifies number of nucleotides at junction that could come from either end of the genome. DI genome type: natural, found during passaging experiments; in silico, designed in silico.